A Symmetric Trefftz-DG Formulation based on a Local Boundary Element Method for the Solution of the Helmholtz Equation

Hélène Barucq, Abderrahmane Bendali, M Fares, Vanessa Mattesi, Sébastien Tordeux

A Symmetric Trefftz-DG Formulation based on a Local Boundary Element Method for the Solution of the Helmholtz Equation

H. Barucq, A. Bendali, M. Fares, V. Mattesi, S. Tordeux

RESEARCH REPORT
N° 8800
October 2015
Project-Team Magique-3D

ISSN 0249-6399 ISRN INRIA/RR--8800--FR+ENG

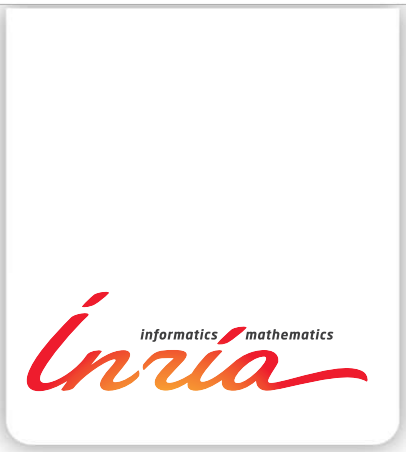

A Symmetric Trefftz-DG Formulation based on a Local Boundary Element Method for the Solution of the Helmholtz Equation

H. Barucq*†, A. Bendali‡§, M. Fares‡, V. Mattesi*‡†, S. Tordeux*†

Project-Team Magique-3D

Research Report n° 8800 — October 2015 — 31 pages

Abstract: A symmetric Trefftz Discontinuous Galerkin formulation, for solving the Helmholtz equation with piecewise constant coefficients, is built by integration by parts and addition of consistent terms. The construction of the corresponding local solutions to the Helmholtz equation is based on a boundary element method. The numerical experiments, which are presented, show an excellent stability relatively to the penalty parameters, and more importantly an outstanding ability of the method to reduce the instabilities known as the "pollution effect" in the literature on numerical simulations of long-range wave propagation.

Key-words: Helmholtz equation, pollution effect, dispersion, Trefftz method, Discontinuous Galerkin method, integral equations, ultra-weak variational formulation, Dirichlet-to-Neumann operator, Boundary Element Method.

* EPC Magique-3D, Pau (France)
† University of Pau (France)
‡ CERFACS, Toulouse (France)
§ University of Toulouse, Mathematical Institute of Toulouse, INSA, Toulouse (France)

RESEARCH CENTRE
BORDEAUX – SUD-OUEST

200 avenue de la Vieille Tour
33405 Talence Cedex

Une formulation symétrique de type Trefftz Galerkine discontinue, à fonctions de forme construites par une méthode d'éléments de frontière, pour la résolution de l'équation d'Helmholtz

Résumé : Une formulation symétrique de type Trefftz Galerkine discontinue, pour la résolution numérique de l'équation de Helmholtz à coefficients constants par morceaux, est construite par intégrations par parties et ajouts de relations vérifiées par consistance. La construction des solutions locales correspondantes de l'équation de Helmholtz est basée sur la méthode des éléments de frontière. Les expériences numériques, présentées dans ce rapport, montrent une excellente stabilité relativement aux paramètres de pénalisation, et surtout une remarquable capacité de la méthode à réduire les instabilités numériques, appelées aussi "pollution numérique" dans la littérature sur les simulations numériques de propagation d'ondes sur de longues distances.

Mots-clés : Équation de Helmholtz, pollution numérique, dispersion, méthode de type Trefftz, méthode Galerkine Discontinue, équations intégrales, formulation variationnelle ultra faible, opérateur de Dirichlet-to-Neumann, méthode éléments de frontière.

Contents

1 Introduction

Usual finite element methods, when used for solving the Helmholtz equation over several hundreds of wavelengths, are faced with the drawback generally called "pollution effect". Roughly speaking, it is necessary to augment the density of nodes to maintain a given level of accuracy, when increasing the size of the computational domain. This in turn rapidly exceeds the capacities in storage and computing even in the framework of massively parallel computer platforms (cf., for example, [29, 15, 33] and the references therein).

Several approaches have been proposed to cure this flaw. At first, for such kinds of numerical solutions, it became well-established that Discontinuous Galerkin (DG) methods are more efficient than standard Finite Element Methods (FEM), also called Continuous Galerkin (CG) methods in this context. This efficiency seems to be due in part to the less strong inter-element continuity characterizing these methods (cf., for example, [1, 2]). Indeed this was confirmed in [32] where it is shown that it is possible to keep the efficiency of the DG methods by allowing discontinuities only at the interior of the elements in terms of bubble functions with penalized jumps.

Another advantage of the above kind of methods lies in the possibility to use shape functions, more adapted to the approximation of the solution to the interior Partial Differential Equations (PDE) of the problem, but, contrary to polynomials, with poor properties for enforcing the usual inter-element continuity conditions of the FEM. In this respect, Trefftz methods, that is, methods for which the local shape functions are wave functions, i.e., solutions to the Helmholtz equation (cf., for example, [22, 38] and the references therein), were intensively used to alleviate the aforementioned "pollution effect". The combination of a Trefftz and a DG method therefore resulted on numerous approaches for solving wave equation problems called Trefftz DG method (TGD) (see, for example, [20, 24, 23, 22] and the references therein).

Actually, Trefftz methods without strong inter-element continuity were used for some time in the context of the so called Ultra Weak Variational Formulation (UWVF) devised by Després [13, 10]. It was discovered later that this formulation can be recast in the context of a TDG method [16, 7, 20] at least for the two latter references when using explicit local solutions to the Helmholtz equations.

Some criticisms have been however addressed to the DG methods. They mainly concern the increase of the coupled degrees of freedom and a suboptimal convergence of their approximate fluxes. Hybridized versions of the DG (HDG) methods were proposed in response to these challenges [12]. However at the authors knowledge, HDG methods have not been used yet in the framework of a Trefftz method but only with usual local polynomial approximations [18], except in a recent paper [36], where these methods were combined in an elaborate way with geometrical optics at the element level to efficiently solve the Helmholtz equation in the high frequency regime. Since the local shape functions are only asymptotic solutions to the Helmholtz equation then, such a kind of method can be called quasi-Trefftz HDG.

Instead of DG methods, some authors prefer to use a Lagrange multiplier or a least-square technique to enforce the continuity conditions (cf. [3, 17, 43]). This is not the approach retained in this paper.

On the other hand, it is generally admitted that Boundary Integral Equations (BIEs) lead to less "pollution effects" than FEMs even if at the authors knowledge no formal study confirming such a property seems to have been already provided. Such a good behavior is probably due to the fact that BIEs can be seen as particular Trefftz methods when such an interpretation is taken to the extreme. It is hence tempting to use the free space Green kernel in an approximation procedure for the interior Helmholtz equation to reduce the "pollution effects". This way to proceed has been already considered in [8]. However it seems hard to extend it to problems

involving varying coefficients or realistic geometries and boundary conditions. The aim of this study is precisely to mix two approaches: DG methods and BIEs, to devise a TDG method which can efficiently handle particular Helmholtz equations with varying coefficients. Specifically, either the coefficients are piecewise constant or they can be approximated in this manner on a sufficiently refined decomposition of the computational domain, called interior mesh in the rest of this paper.

The method can be viewed globally as a DG method at the level of the interior mesh and as a BIE locally at the element level. Actually, BIEs are used only to compute the Dirichlet-to-Neumann (DtN) operator within each element of the interior mesh. As shown below, the quality of the overall solution strongly depends on the accuracy of the approximation of this operator. Specific numerical procedures have therefore been developed to increase the accuracy of this approximation. Such a treatment can be related to similar techniques developed in [26, 14].

The method proposed in this study owns other additional interesting properties. As a DG method, it is formulated as a symmetric DG method, that is, as a symmetric variational formulation of the corresponding boundary-value problem. Its derivation follows the path devised in [4] (see also [37, p. 122]) for designing Symmetric Interior Penalty (SIP) methods but in a bit different way, more straightforward in our opinion. Additionally, when the penalty terms enforcing the continuity of the normal traces (really the dual variables) are discarded, this symmetry here yields an important gain. The storage of the boundary integral operators involved in the formulation is then avoided: the contribution of the BIEs then being element-wise only. It is also worth noting that all the degrees of freedom of the discrete problem to be solved are located on the skeleton of the mesh, that is, the boundaries of the elements. Such a feature is characteristic to the reduction of unknowns yielded by HDG methods even if here there still remains unknowns on both sides of the interfaces. "Last but not least" perhaps the most important advantage of the proposed approach lies on the choice of the local shape functions which account for all kinds of waves: evanescent, propagative, etc. This is in contrast with usual Trefftz methods which locally use plane, circular/spherical waves, multipoles, etc. (cf., for example, [3, 23, 34, 20, 10] to cite a few). It should be noted also that, even if the method, which is considered here, is of Trefftz type, the local approximations are done by means of a Boundary Element Method (BEM) (cf., for example, [40, 6]). As a result, these approximations are ultimately performed in terms of piecewise polynomial functions on a BEM mesh. In contrast then to usual Trefftz methods, h or p refinements are as simple and efficient as in a standard FEM. This is why this method is called the BEM Symmetric Trefftz DG method in the succeeding text and more concisely denoted by BEM-STDG.

The paper is organized as follows. In Section 2, after stating the boundary-value problem, we first derive the variational formulation of the symmetric TDG method and show how it can be connected to previous DG formulations. Section 3 develops the BEM procedure used to define the Trefftz method. Section 4 is devoted to the numerical validation of the method in two dimensions and to the comparison of its performances with a standard Interior Penalty DG (IPDG) method based on element-wise polynomial approximations. A final brief section gives some concluding remarks and indicates further studies that can extend this one.

2 The symmetric Trefftz DG method

After stating the wave propagation problem, we describe the most general DG formulation considered in this study.

2.1 The Helmholtz boundary-value problem

The DG variational formulations of the Helmholtz equation (cf., for example, [22, 20, 24]) are generally obtained by writing the wave equation in the form of a first-order PDEs system. Most of the studies dedicated to the solution of this problem by this kind of techniques (in addition to the previous references, see, for example, [10, 7, 42, 33]) deal with the Helmholtz equation with constant coefficients. If acoustics is taken as the concrete shape to the problem being dealt with, this amounts to assuming that the equations governing the acoustic fluctuations of pressure and velocity correspond to the propagation of an acoustic wave in an ideal stagnant and uniform fluid (cf., for example. [39, Chap. 2]). We follow here a more general path and consider as in [28] that the propagation is related to an ideal stagnant fluid but not necessarily uniform. The acoustic system for such a configuration can be written as follows (cf., for example, [31, Eqs. (64.5) and (64.3)])

$$\left\{ \begin{array}{l} \frac{1}{c^2\varrho}\partial_t p + \nabla \cdot \boldsymbol{v} = 0, \\ \varrho \partial_t \boldsymbol{v} + \nabla p = 0, \end{array} \right. \tag{1}$$

where c and ϱ are the speed of sound and the density within the stagnant fluid and p and $\boldsymbol{v}$ are respectively the acoustic fluctuations of the pressure and the velocity. Hereafter data c and ϱ are assumed to be piecewise constant. As this will be clear below, the handling of the related discontinuities is an important part of the DG formulation.

To be consistent with the notation used in previous works [22, 20, 24, 42, 33], we denote the phasors of respectively the pressure and the velocity by a different symbol: u for p defined according to the following identities and characterizations

$$p(x,t) = \Re\left(e^{-i\omega t}u(x)\right), \quad \boldsymbol{v}\left(x,t\right) = \Re\left(e^{-i\omega t}\boldsymbol{\sigma}\left(x\right)\right). \tag{2}$$

In the above definitions, $\Re z$ is the real part of the complex number z, and $\omega > 0$ is the angular frequency. The solution of (1) is hence reduced to

$$\left\{ \begin{array}{l} -\frac{i\omega}{c^2\varrho}u + \nabla \cdot \boldsymbol{\sigma} = 0, \\ -i\omega\varrho\boldsymbol{\sigma} + \nabla u = 0. \end{array} \right. \tag{3}$$

We now assume that the equations are set in a bounded polygonal/polyhedral domain $\Omega \subset \mathbb{R}^d$ ($d = 2, 3$) and denote by $\partial\Omega$ its boundary. Using the piecewise constant wave number $\kappa = \omega/c$, and considering a non overlapping decomposition $\partial\Omega_D$, $\partial\Omega_N$, and $\partial\Omega_R$ of $\partial\Omega$, we recast the above system as the following Helmholtz equation with varying coefficients supplemented with typical boundary conditions

$$\left\{ \begin{array}{ll} \boldsymbol{\nabla} \cdot \frac{1}{\varrho}\boldsymbol{\nabla} u + \frac{\kappa^2}{\varrho}u = 0 & \text{in } \Omega, \\ u = g_D & \text{on } \partial\Omega_D, \\ \frac{1}{\varrho}\boldsymbol{\nabla} u \cdot \boldsymbol{n} = g_N & \text{on } \partial\Omega_N, \\ \frac{1}{\varrho}\boldsymbol{\nabla} u \cdot \boldsymbol{n} - iYu = g_R & \text{on } \partial\Omega_R. \end{array} \right. \tag{4}$$

The third boundary condition is expressed in terms of a function Y yielding the surface compliance of $\partial\Omega_R$ up to a multiplicative constant, assumed to be also piecewise constant. The sources producing the wave are embodied in the right-hand sides g_D, g_N and g_R. We have denoted by $\boldsymbol{n}$ the unit normal on $\partial\Omega$ directed outwards Ω (see FIG. 1).

Under minimal assumptions on the geometry of Ω, on κ, ϱ, and Y, on the right-hand sides g_D, g_N and g_R, and assuming furthermore for example that $\Re Y \geq \nu > 0$ on a part of $\partial\Omega_R$ with a non vanishing length/area, it is well-known that problem (4) admits one and only one solution in an adequate functional setting (cf., for example, [35, 44]).

The Helmholtz equation with varying coefficients in system (4) is exactly the wave equation considered in [28]. The boundary condition has been taken there in the following form

$$\frac{1}{\varrho}\partial_{\mathbf{n}}u - i\eta u = Q\left(-\frac{1}{\varrho}\partial_{\mathbf{n}}u - i\eta u\right) + g \tag{5}$$

with $\eta = \kappa/\varrho$ and Q and g given here by

$$\begin{cases} Q = -1, & g = -2i\eta g_D, & \text{on } \partial\Omega_D, \\ Q = +1, & g = 2g_N, & \text{on } \partial\Omega_N, \\ Q = (1 - Y/\eta)\,/\,(1 + Y/\eta)\,, & g = (1+Q)g_R, & \text{on } \partial\Omega_R, \end{cases} \tag{6}$$

thus expressing the three boundary conditions in (4) in a single one. This is more than another way of writing the boundary conditions. It makes it possible to express the "incoming wave" $(1/\varrho)\partial_{\mathbf{n}}u - i\eta u$ in terms of a reflection of the "outgoing wave" $Q\,(-(1/\varrho)\partial_{\mathbf{n}}u - i\eta u)$ and a source term g.

It is worth noting however that Helmholtz equation is involved in other kinds of wave propagation problems. An important example of these is related to seismic waves where attenuation effects must be accounted for in addition to the propagation features. The Helmholtz equation governing this kind of waves is in the following form [41]

$$\Delta u + \frac{\varrho\omega^2}{E}u = 0 \tag{7}$$

where ϱ and ω are the density and the angular frequency and E is the complex modulus. Clearly this equation can be put in the above setting by substituting $1/c^2$ for ϱ/E and ϱ for 1 in system (3). This leads thus to a complex wave number κ. Since we are interested mainly in this paper on accurately accounting for long-range propagation, we limit ourselves below to real coefficients.

2.2 The variational formulation

2.2.1 The interior mesh

At first, we consider a non overlapping decomposition $\mathcal{T}$ of Ω in polyhedral/polygonal subdomains of the computational domain Ω, called the interior mesh as said in the introduction. Considering that the elements $T \in \mathcal{T}$ are open sets of $\mathbb{R}^d$, we therefore assume that

$$\overline{\Omega} = \bigcup_{T\in\mathcal{T}} \overline{T}, \qquad T \cap L = \varnothing \quad \text{if } T \neq L.$$

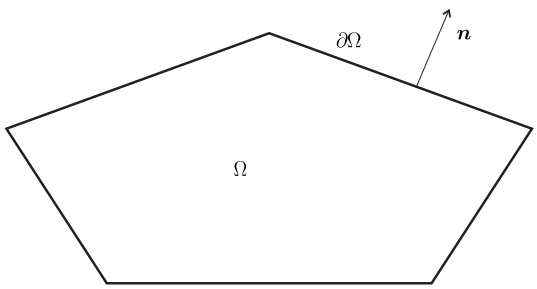

Figure 1: Schematic view of the computational domain.

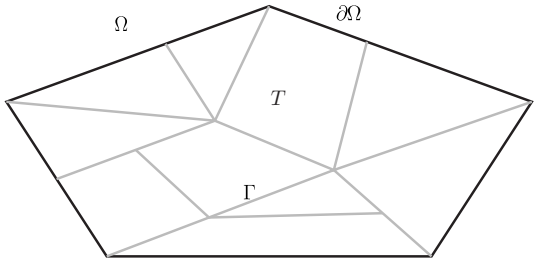

Figure 2: Interior mesh in 2D.

It is worth recalling that this interior mesh can be quite arbitrary. Such a mesh in the two-dimensional case is depicted in FIG. 2.

We always assume that the coefficients ϱ and κ of the Helmholtz equation are real positive constants within each $T \in \mathcal{T}$ and denoted there by ϱ_T and κ_T respectively.

2.2.2 Interior and boundary faces

We pass to the definition of interior and boundary edges/faces on which is based the setting of any DG method. Interior edges/faces F are part of the boundary ∂T of $T \in \mathcal{T}$ shared by another $L \in \mathcal{T}$. They are defined as follows

$$F = \partial T \cap \partial L \text{ when the length/area of } F \text{ is } > 0. \tag{8}$$

Some other definitions characterize F by requiring that it contains at least d points constituting a non degenerated simplex (segment and triangle in the two- and the three-dimensional case respectively) [4]. Boundary edges/faces F are defined similarly by replacing L with the exterior of Ω. We use a set notation $\mathcal{F}_\mathcal{I}$ and $\mathcal{F}_\partial$ to refer to the collections of interior and boundary edges/faces respectively. Clearly the interior edges/faces F constitute a non-overlapping decomposition of the following curve/surface

$$\Gamma = \bigcup_{F \in \mathcal{F}_\mathcal{I}} F.$$

In the same way, the boundary edges/faces yield a non-overlapping decomposition of $\partial\Omega$

$$\partial\Omega = \bigcup_{F \in \mathcal{F}_\partial} F.$$

In FIG. 2, Γ is depicted in grey while $\partial\Omega$ is in black.

2.2.3 Traces and Green formula

Assuming that the solution u to problem (4) and the test function v are piecewise smooth, we can use the usual Green formula to get

$$\begin{aligned}\sum_{T\in\mathcal{T}}\int_T \left(\tfrac{1}{\varrho_T}\boldsymbol{\nabla} u\cdot\boldsymbol{\nabla} v - \tfrac{\kappa_T^2}{\varrho_T}uv\right) dx \\ &= \sum_{T\in\mathcal{T}}\int_T \left(\tfrac{1}{\varrho_T}\boldsymbol{\nabla} u\cdot\boldsymbol{\nabla} v + v\boldsymbol{\nabla}\cdot\tfrac{1}{\varrho_T}\boldsymbol{\nabla} u\right) dx \\ &= \sum_{T\in\mathcal{T}}\int_{\partial T} \left(\tfrac{1}{\varrho}\boldsymbol{\nabla} u\right)|_{\partial T}\cdot\boldsymbol{n}_T v_T ds\end{aligned} \tag{9}$$

with

$$v_T = v|_{\partial T} \tag{10}$$

the traces being taken from the values of v inside T. Vector $\boldsymbol{n}_T$ is the unit normal to ∂T directed outwards T. Actually below, we can take advantage of the fact that the normal component of $1/\varrho\boldsymbol{\nabla}u$ is continuous across F to write the sum of the integrals on each ∂T in the following manner

$$\sum_{T\in\mathcal{T}}\int_{\partial T}\left(\frac{1}{\varrho}\boldsymbol{\nabla}u\right)|_{\partial T}\cdot\boldsymbol{n}_T v_T ds = \sum_{F\in\mathcal{F}_\mathcal{I}}\int_F \frac{1}{\varrho}\boldsymbol{\nabla}u\cdot[\![v]\!]ds + \sum_{F\in\mathcal{F}_\partial}\int_F \frac{1}{\varrho}\boldsymbol{\nabla}u\cdot\boldsymbol{n}vds \tag{11}$$

using the widespread notation (cf., for example, [5]) for the jump of v across F

$$[\![v]\!] = \boldsymbol{n}_T v_T + \boldsymbol{n}_L v_L, \tag{12}$$

T and L being the two elements of the mesh sharing edge/face F.

It is a part of the derivation of the variational formulation of the DG method to express the continuity of the normal component of $1/\varrho\boldsymbol{\nabla}u$ across any edge/face F from the mean of its traces on both sides of F

$$\{\!\{\frac{1}{\varrho}\nabla u\}\!\} = \frac{1}{2}\left(\left(\frac{1}{\varrho}\nabla u\right)|_T + \left(\frac{1}{\varrho}\nabla u\right)|_L\right) \tag{13}$$

thus arriving to

$$\sum_{T\in\mathcal{T}}\int_T \frac{1}{\varrho_T}\left(\boldsymbol{\nabla}u\cdot\boldsymbol{\nabla}v - \kappa_T^2 uv\right)dx = \int_\Gamma \{\!\{\frac{1}{\varrho}\nabla u\}\!\}\cdot[\![v]\!]ds + \int_{\partial\Omega}\frac{1}{\varrho}\boldsymbol{\nabla}u\cdot\boldsymbol{n}vds. \tag{14}$$

The above expression of $\{\!\{1/\varrho\nabla u\}\!\}\cdot[\![v]\!]$ must be understood in the meaning of the normal traces since only these quantities can really be defined in the weak formulation of problem (4) and are involved in the TDG method.

2.2.4 General variational formulation of the symmetric Trefftz-DG method

In the same way, assuming now that test function v is an element-wise solution to the Helmholtz equation

$$\Delta v + \kappa_T^2 v = 0 \text{ in } T \qquad (T\in\mathcal{T}),$$

and using the fact this once that it is the unknown u which is continuous across the interfaces F, we can write

$$\sum_{T\in\mathcal{T}}\int_T \frac{1}{\varrho_T}\left(\boldsymbol{\nabla}u\cdot\boldsymbol{\nabla}v - \kappa_T^2 uv\right)dx = \int_\Gamma u[\![\frac{1}{\varrho}\nabla v]\!]ds + \int_{\partial\Omega} u\frac{1}{\varrho}\boldsymbol{\nabla}v\cdot\boldsymbol{n}\ ds \tag{15}$$

where as usual (cf., for example, [5]) the jump $[\![1/\varrho\nabla v]\!]$ is defined by

$$[\![\frac{1}{\varrho}\nabla v]\!] = \left(\frac{1}{\varrho}\nabla v\right)|_T\cdot\boldsymbol{n}_T + \left(\frac{1}{\varrho}\nabla v\right)|_L\cdot\boldsymbol{n}_L. \tag{16}$$

In the same way as above for $1/\varrho\boldsymbol{\nabla}u$, we substitute the mean value

$$\{\!\{u\}\!\} = \frac{1}{2}\left(u_T + u_L\right), \tag{17}$$

for the trace of u and use (14) to obtain the following variational equation set on the edges/faces of the interior mesh

$$\int_\Gamma \left(\{\!\{u\}\!\} [\![\frac{1}{\varrho} \nabla v]\!] - \{\!\{ \frac{1}{\varrho} \nabla u \}\!\} \cdot [\![v]\!] \right) ds + \int_{\partial\Omega} \left(u \frac{1}{\varrho} \nabla v \cdot \boldsymbol{n} - \frac{1}{\varrho} \nabla u \cdot \boldsymbol{n} v \right) ds = 0. \tag{18}$$

To design a symmetric formulation, we proceed as in [4, 15] (see also [37, p. 122]). We make use of the following interior identities

$$[\![u]\!] = 0 \quad \text{and} \quad [\![\frac{1}{\varrho} \nabla u]\!] = 0 \tag{19}$$

and the boundary conditions to add some consistent terms to Eq. (18) thus arriving to

$$\begin{aligned} &\int_\Gamma \left(\{\!\{u\}\!\} [\![\tfrac{1}{\varrho} \nabla v]\!] + [\![\tfrac{1}{\varrho} \nabla u]\!] \{\!\{v\}\!\} - \{\!\{ \tfrac{1}{\varrho} \nabla u \}\!\} \cdot [\![v]\!] - [\![u]\!] \{\!\{ \tfrac{1}{\varrho} \nabla v \}\!\} \right) ds \\ &\quad - \int_{\partial\Omega_D} \left(u \tfrac{1}{\varrho} \nabla v \cdot \boldsymbol{n} + \tfrac{1}{\varrho} \nabla u \cdot \boldsymbol{n} v \right) ds \\ &\quad + \int_{\partial\Omega_N \cup \partial\Omega_R} \left(u \tfrac{1}{\varrho} \nabla v \cdot \boldsymbol{n} + \tfrac{1}{\varrho} \nabla u \cdot \boldsymbol{n} v \right) ds + 2 \int_{\partial\Omega_R} (-iY)\, uv ds \\ &\quad = -2 \int_{\partial\Omega_D} g_D \tfrac{1}{\varrho} \nabla v \cdot \boldsymbol{n} ds + 2 \int_{\partial\Omega_N} g_N v ds + 2 \int_{\partial\Omega_R} g_R v ds. \end{aligned} \tag{20}$$

To stabilize the formulation, in view of already known DG methods [5, 20, 15], we finally add consistent penalty terms expressed by means of given functions α, β, γ and δ defined on Γ and $\partial\Omega$. In this way, we arrive to the following most general variational formulation on which are based the TDG methods considered in this paper

$$a(u, v) = Lv \tag{21}$$

where a is the following symmetric bilinear form

$$\begin{aligned} a(u,v) = &\int_\Gamma \left(\{\!\{u\}\!\} [\![\tfrac{1}{\varrho} \nabla v]\!] + [\![\tfrac{1}{\varrho} \nabla u]\!] \{\!\{v\}\!\} - \{\!\{ \tfrac{1}{\varrho} \nabla u \}\!\} \cdot [\![v]\!] - [\![u]\!] \cdot \{\!\{ \tfrac{1}{\varrho} \nabla v \}\!\} \right) ds \\ &+ \int_\Gamma \left(\alpha [\![u]\!] [\![v]\!] + \beta \nabla_\top [\![u]\!] \odot \nabla_\top [\![v]\!] + \gamma [\![\tfrac{1}{\varrho} \nabla u]\!] [\![\tfrac{1}{\varrho} \nabla v]\!] \right) ds \\ &- \int_{\partial\Omega_D} \left(u \tfrac{1}{\varrho} \nabla v \cdot \boldsymbol{n} + \tfrac{1}{\varrho} \nabla u \cdot \boldsymbol{n} v \right) ds \\ &+ \int_{\partial\Omega_N \cup \partial\Omega_R} \left(u \tfrac{1}{\varrho} \nabla v \cdot \boldsymbol{n} + \tfrac{1}{\varrho} \nabla u \cdot \boldsymbol{n} v \right) ds - 2 \int_{\partial\Omega_R} iY uv ds \\ &+ \int_{\partial\Omega_D} (\alpha uv + \beta \nabla_\top u \nabla_\top v)\, ds + \int_{\partial\Omega_N} \delta \tfrac{1}{\varrho} \nabla u \cdot \boldsymbol{n}\ \tfrac{1}{\varrho} \nabla v \cdot \boldsymbol{n} ds \\ &+ \int_{\partial\Omega_R} \delta \left(\tfrac{i}{Y} \tfrac{1}{\varrho} \nabla u \cdot \boldsymbol{n} \tfrac{1}{\varrho} \nabla v \cdot \boldsymbol{n} + \tfrac{1}{\varrho} \nabla u \cdot \boldsymbol{n}\ v + u \tfrac{1}{\varrho} \nabla v \cdot \boldsymbol{n} - iY uv \right) ds, \end{aligned} \tag{22}$$

and where the right-hand side is defined by

$$\begin{aligned} Lv = &\int_{\partial\Omega_D} \left(-2 g_D \tfrac{1}{\varrho} \nabla v \cdot \boldsymbol{n} + \alpha g_D v + \beta \nabla_\top g_D \nabla_\top v \right) ds \\ &+ \int_{\partial\Omega_N} \left(2 g_N v + \delta g_N \tfrac{1}{\varrho} \nabla v \cdot \boldsymbol{n} \right) ds + \int_{\partial\Omega_R} 2 g_R v + \delta g_R \left(\tfrac{i}{Y} \tfrac{1}{\varrho} \nabla v \cdot \boldsymbol{n} + v \right) ds. \end{aligned} \tag{23}$$

In the above expressions, $\nabla_\top u$ is the tangential gradient of u whereas $\nabla_\top [\![u]\!] \odot \nabla_\top [\![v]\!]$ is defined by

$$\begin{aligned}\nabla_\top [\![u]\!] \odot \nabla_\top [\![v]\!] &= \nabla_\top (u_T - u_L) \cdot \nabla_\top (v_T - v_L) \\ &= \nabla_\top (u_L - u_T) \cdot \nabla_\top (v_L - v_T)\end{aligned}$$

on any interior edge/face F shared by elements T and L.

2.3 Comparison with previous Trefftz-DG formulations

A thorough review of Trefftz methods for solving the Helmholtz equation has been recently performed in [22]. We limit ourselves here to a comparison with methods of DG type. The following clear definition of such a kind of methods is given in this reference: *"DG"* [...] [are] *methods that arrive at local variational formulation by applying integration by parts to the PDE to be approximated.*

2.3.1 Comparison with Interior Penalty DG Methods

Interior Penalty DG (IPDG) methods are mostly introduced as above by integration by parts at the element level and adding consistent penalty terms (see for instance [4, 15, 37] and the references therein).

Actually adapting the IPDG introduced in [4] to the Helmholtz equation involved in (4) and considering that $\partial\Omega_D = \partial\Omega$ as in this reference, we obtain

$$\begin{aligned}&\sum_{T\in\mathcal{T}} \int_T \tfrac{1}{\varrho_T} \left(\boldsymbol{\nabla} u \cdot \boldsymbol{\nabla} v - \kappa_T^2 uv\right) dx \\ &\quad - \int_\Gamma \left(\{\!\{ \tfrac{1}{\varrho} \nabla u \}\!\} \cdot [\![v]\!] + [\![u]\!] \{\!\{ \tfrac{1}{\varrho} \nabla v \}\!\} \right) ds - \int_{\partial\Omega_D} \left(u \tfrac{1}{\varrho} \nabla v \cdot \boldsymbol{n} + \tfrac{1}{\varrho} \nabla u \cdot \boldsymbol{n} v \right) ds \\ &\quad + \int_\Gamma \alpha [\![u]\!] \cdot [\![v]\!] \, ds + \int_{\partial\Omega_D} \alpha uv \, ds = \int_{\partial\Omega_D} \left(-g_D \tfrac{1}{\varrho} \nabla v \cdot \boldsymbol{n} + \alpha g_D v \right) ds.\end{aligned}$$

Using the fact that v is also a solution to the Helmholtz equation in T and integrating by parts once again, we get

$$\begin{aligned}&\int_\Gamma \left(u [\![\tfrac{1}{\varrho} \nabla v]\!] - \{\!\{ \tfrac{1}{\varrho} \nabla u \}\!\} \cdot [\![v]\!] - [\![u]\!] \{\!\{ \tfrac{1}{\varrho} \nabla v \}\!\} \right) ds \\ &\quad + \int_{\partial\Omega_D} u \tfrac{1}{\varrho} \nabla v \cdot \boldsymbol{n} ds - \int_{\partial\Omega_D} \left(u \tfrac{1}{\varrho} \nabla v \cdot \boldsymbol{n} + \tfrac{1}{\varrho} \nabla u \cdot \boldsymbol{n} v \right) ds + \int_{\partial\Omega_D} \alpha uv \, ds \\ &\quad + \int_\Gamma \alpha [\![u]\!] \cdot [\![v]\!] \, ds = \int_{\partial\Omega_D} \left(-g_D \tfrac{1}{\varrho} \nabla v \cdot \boldsymbol{n} + \alpha g_D v \right) ds.\end{aligned}$$

Using the equivalent expressions

$$\int_\Gamma u [\![\frac{1}{\varrho} \nabla v]\!] ds = \int_\Gamma \{\!\{u\}\!\} [\![\frac{1}{\varrho} \nabla v]\!] ds \text{ and } \int_\Gamma [\![\frac{1}{\varrho} \nabla u]\!] \{\!\{v\}\!\} ds = 0$$

and substituting g_D for u in the first integral on $\partial\Omega_D$, we directly arrive to formulation (21) with $\beta = \gamma = 0$.

Proceeding in the same way for the IPDG method considered in [15], we find again formulation (21) with $Y = -\kappa$, $g_D = 0$, $\delta = 0$, $\partial\Omega_N = \varnothing$.

It is clear from the above examples that, up to some consistent terms, any IPDG method can be put in the form of variational formulation (21) with suitable values for the penalty parameters α, β, δ, and γ.

2.3.2 Comparison with DG methods based on numerical fluxes

Two broad classes, in which can be split the DG methods based on numerical fluxes for the Helmholtz equation, likely first come to mind: those which are a simple reformulation of the above IPDG methods and those which can be linked to an upwinding numerical scheme. Actually, in the context of the solution of the Helmholtz equation, the upwinding techniques are intimately related to the UWVF as this was brought out in [16]. However, in the authors opinion, upwinding is stated in the literature in a clear manner only for the Helmholtz equation with constant coefficients. We found it useful to recall some features about these techniques to more clearly set out the difference between a real upwind scheme and a simple enforcement of the continuity conditions when the PDE coefficients are discontinuous.

The starting point is the use of either of the following techniques performed in every element T of the interior mesh:

- **the primal method**, as it is called in [20], which consists in integrating by parts the Helmholtz equation with the additional feature that v is a solution to the local Helmholtz equation,
- **the mixed method** [24], where the integration by parts is carried out on a first-order system, which is an equivalent formulation of the Helmholtz equation with a pairing $(v, \boldsymbol{\tau})$ solution to the complex conjugate system (this can also be done without reference to the scalar equation, directly on system (3), in [16]).

Both of these approaches give rise to the following variational equation

$$\int_{\partial T} (\widehat{\boldsymbol{\sigma}} \cdot \boldsymbol{n}_T v_T + \widehat{u} \boldsymbol{n}_T \cdot \boldsymbol{\tau})\, ds = 0 \tag{24}$$

where, without further steps being taken, $\widehat{\boldsymbol{\sigma}} = \boldsymbol{\sigma}_T$ and $\widehat{u} = u_T$ (see [42] also).

In a series of papers (cf. [22] and the references therein), Hiptmair, Moiola, Perugia, and their co-authors obtained variational formulation (21) without the consistent terms added to the above IPDG methods to get a symmetric variational formulation. It is worth mentioning that the variational formulation used in these studies is not symmetric. It can lead however to a symmetric linear system if the involved edge/face integrals are calculated exactly.

2.3.3 The upwinding scheme

It is also shown in the above papers (see also [7]) that, for the Helmholtz equation with constant coefficients, the UWVF can be recast in the framework of the above TDG method for particular values of α, β, γ and δ. Formulation (21) can hence be viewed as a symmetric variational extension of the UWVF method if the specific properties of the UWVF, related to the fact that it can be posed in terms of a perturbation of the identity by a norm dimunishing operator, are discarded [10]. However, one must be aware that then this formulation can no longer be considered as an upwinding scheme. In the same way, the extension given in [28] for boundary-value problem (4) for piecewise constant coefficients, can still be understood as a UWVF or can be recast as Trefftz DG method but not exactly as an upwinding scheme. Actually, this extension can be interpreted as a centered method for designing a local homogeneous propagation environment first and using a upwinding scheme then. A similar handling of discontinuous coefficients is standard in the numerical solution of time domain hyperbolic systems. A nice presentation of this technique is given in [21]. Indeed, it is shown in [9] that the medium, in which the wave is propagating, can be set arbitrarily before performing the upwinding scheme while keeping the

general properties of the UWVF. A clear connection, at least for an homogeneous medium of propagation, between the UWVF and an upwinding scheme based on a way to express matching conditions (19) equivalently as a balance sheet of the incoming and outgoing waves crossing an edge/face, is given in [16].

3 The BEM symmetric Trefftz DG method

We first use a boundary integral equation approach to express the "dual variables"

$$p_T = \left(\frac{1}{\varrho_T}\nabla u\right)|_T \cdot \boldsymbol{n}_T \text{ and } q_T = \left(\frac{1}{\varrho_T}\nabla v\right)|_T \cdot \boldsymbol{n}_T \tag{25}$$

from the traces u_T and v_T of u and v on ∂T respectively. The BEM-STDG method can then be fully derived from a boundary element approximation of u_T, v_T, p_T, and q_T for $T \in \mathcal{T}$.

3.1 The boundary integral equation within each element of the interior mesh

For the moment, we assume that the interior Dirichlet problem is well-posed within any $T \in \mathcal{T}$. A geometrical criterion ensuring this property is given below. As a result, the single-layer boundary integral operator defined for sufficiently smooth p_T by

$$V_T p_T(x) = \int_{\partial T} G_T(x,y) p_T(y) ds_y \quad (x \in \partial T) \tag{26}$$

is invertible. From the well-known integral representations of the solutions to the Helmholtz equation with constant coefficients, it then results that the above traces u_T and $p_T = 1/\varrho_T \nabla u \cdot \boldsymbol{n}_T$ are linked as follows

$$V_T p_T = \frac{1}{\varrho_T}\left(\tfrac{1}{2} - N_T\right) u_T \tag{27}$$

where N_T is the double-layer boundary integral operator

$$N_T u_T(x) = -\int_{\partial T} \partial_{\boldsymbol{n}_T(y)} G_T(x,y) u_T(y) ds_y \quad (x \in \partial T)\,. \tag{28}$$

The kernel $G_T(x,y)$ involved in the above formulas is that corresponding to the outgoing solutions to the Helmholtz equation with wavenumber κ_T. For all these properties related to the solution of Helmholtz equation by boundary integral equations, we refer for instance to [35, 25, 6].

We now turn our attention to the abovementioned geometric criterion. It is stated as follows.

Geometric criterion. *Assume that there exists a unit vector $\boldsymbol{\upsilon}$ such that*

$$\sup\,(x-y)\cdot\boldsymbol{\upsilon} \le \lambda_T/2 \text{ for all } x \text{ and } y \text{ in } T, \tag{29}$$

where $\lambda_T = 2\pi/\kappa_T$ is the wavelength within T. Then, the boundary-value problem for the Helmholtz equation with Dirichlet boundary condition and wavenumber κ_T is well posed in T.

Set $\ell = \sup\,(x-y)\cdot\boldsymbol{\upsilon}$. With no loss of generality, we can assume that $T \subset]0,\ell[\times \prod_{i=2,\ldots,d}]0,\ell_i[$. From the min max principle, it can be argued that the first eigenvalue χ^2 of the Laplace operator with a Dirichlet boundary condition satisfies $\chi^2 \ge \pi^2/\left(\ell^2+\ell_2^2+\cdots+\ell_d^2\right)$, thus establishing the criterion since $\ell \le \lambda_T/2$, and therefore $\kappa_T \le \pi/\ell < \chi$.

3.2 The BEM symmetric Trefftz DG method

3.2.1 The local boundary element method

Actually, only the interfaces $F \in \mathcal{F}_\mathcal{I}$ shared by two elements of the interior mesh or those $F \in F_\partial$ limiting the exterior of the computational domain, in other words the skeleton of the interior mesh, have to be meshed. This is perhaps a first important feature of the method: it is a TDG method but also turns out to be a BEM at the element level. It is therefore possible to carry out a refinement of the skeleton mesh, that is, the mesh accounting for the accuracy of the local approximating functions, without any modification of the interior mesh.

Actually, it is possible to use a BEM with no matching condition and thus to benefit from the advantage of meshing the various faces F each independently of the other. However, we have observed from several numerical experiments that a higher accuracy is reached for continuous approximations of u_T and v_T respectively, of course with no inter-element continuity condition. This is not at all restrictive in the two-dimensional case but makes it necessary to mesh each face F according to the usual matching conditions of a continuous FEM within the boundary ∂T of T in three dimensions (cf., for example, [11, 30]). The resulting mesh is called the skeleton mesh in the succeeding text. Any function u_T or v_T is sought as a polynomial function of degree m, that is, in $\mathbb{P}_m$, within each element of the skeleton mesh, continuous on ∂T but with no further continuity condition as said above. A clear idea on the continuity conditions that are imposed on the considered element-wise BEM is given in FIG. 3. For clarity, the boundary nodes on the various faces are represented inside the elements of the interior mesh. A same marker for the nodes is used to indicate the continuity conditions imposed on the boundary traces of the shape functions.

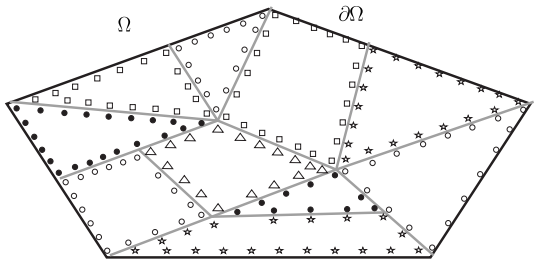

Figure 3: Skeleton mesh and nodes used in the 2D case.

3.2.2 Approximation of the dual variables

The involvement of the BEM at the level of the TDG method is completely embodied in the approximation of the DtN operator expressing the dual variable p_T in terms of u_T by solving Eq. (27). The accuracy of this approximation is crucial for the reduction of the "pollution effect". To enhance the sharpness of this procedure, we have adopted the following strategy:

- u_T is approximated on the skeleton mesh and p_T on a refined mesh obtained by subdividing each of the elements of the former;
- contrary to u_T, p_T is continuous within each edge/face only, but not at the junctions of the edges/faces;

Let us denote by $[u_T]$, $\left[p_T^\#\right]$, $[v_T]$, $\left[q_T^\#\right]$ the column-wise vector whose components are the nodal values of u_T, p_T, v_T, q_T. We denote also by $\left[u_T^\#\right]$ and $\left[v_T^\#\right]$ the nodal values of u_T and v_T

on the augmented set of nodes obtained either by interpolating u_T and v_T respectively on the refined mesh or by doubling nodes where p_T or q_T are not continuous so that $\left[u_T^{\#}\right]$, $\left[v_T^{\#}\right]$, $\left[p_T^{\#}\right]$, and $\left[q_T^{\#}\right]$ are all of the same length and have components all referring to the same nodes. The components of $\left[u_T^{\#}\right]$ are expressed in terms of those of $[u_T]$ by means of an explicit matrix $[P_T]$

$$\left[u_T^{\#}\right] = [P_T]\,[u_T]\,. \tag{30}$$

Let us then define the matrices $\left[M_T^{\#}\right]$, $\left[V_T^{\#}\right]$, and $\left[N_T^{\#}\right]$ through the following identifications

$$\begin{cases} \left[q_T^{\#}\right]^{\top}\left[M_T^{\#}\right]\left[p_T^{\#}\right] = \displaystyle\int_{\partial T} p_T q_T ds, \\ \left[q_T^{\#}\right]^{\top}\left[V_T^{\#}\right]\left[p_T^{\#}\right] = \displaystyle\int_{\partial T} (V_T p_T)\, q_T ds, \\ \left[q_T^{\#}\right]^{\top}\left[N_T^{\#}\right]\left[p_T^{\#}\right] = \displaystyle\int_{\partial T} (N_T p_T)\, q_T ds. \end{cases}$$

Equation (27) then yields that nodal values $\left[p_T^{\#}\right]$ and $\left[q_T^{\#}\right]$ are expressed at the level of interior element T by

$$\begin{cases} \left[p_T^{\#}\right] = \left[D_T^{\#}\right]\left[u_T^{\#}\right], \quad \left[q_T^{\#}\right] = \left[D_T^{\#}\right]\left[v_T^{\#}\right], \\ \left[D_T^{\#}\right] = \frac{1}{\varrho_T}\left[V_T^{\#}\right]^{-1}\left(\frac{1}{2}\left[M_T^{\#}\right] - \left[N_T^{\#}\right]\right). \end{cases} \tag{31}$$

It is at this level that the well-posedness of the interior Dirichlet problem for the laplacian enters into the picture. It ensures the invertibility of matrix $\left[V_T^{\#}\right]$.

Using (30), we thus get the approximation of the DtN operator

$$\left[p_T^{\#}\right] = \left[D_T^{\#}\right]\,[P_T]\,[u_T]\,. \tag{32}$$

At this stage, it is important for clarity to recall that the method involves three meshes:

- the interior mesh $\mathcal{T}$ used for setting the BEM-STDG method; each $T \in \mathcal{T}$ must satisfy the above geometric criterion yielding that the local Dirichlet problem is well-posed;
- the skeleton mesh used by the local BEM to set up the local approximating functions which are solutions within each $T \in \mathcal{T}$ of the Helmholtz equation (local wave functions);
- the refined mesh within the boundary ∂T of each $T \in \mathcal{T}$ allowing for an accurate approximation of the DtN operator; this mesh is specified through a positive integer $N_{\rm add}$ yielding the way in which each element of the skeleton mesh is subdivided; for instance, for the numerical experiments in two dimensions performed below, $N_{\rm add}$ is the number of segments in which each segment of the skeleton mesh is subdivided.

A schematic view of these three meshes is displayed in FIG. 4. Note that the global nodal values correspond to the nodes of the skeleton mesh (vertices of the skeleton mesh when using a BEM with local shape functions that are polynomials of degree $m = 1$) and that the nodes related to the refined mesh are only used in element-wise computations.

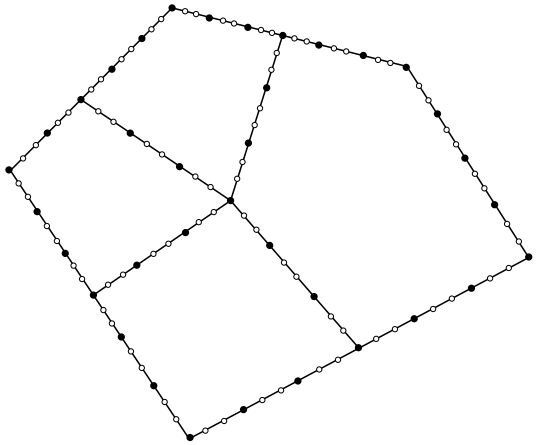

Figure 4: Schematic view of the three kinds of meshes, which are used in the BEM-STDG method. The 4 polygonals constitute the interior mesh. The vertices of the skeleton and the refined meshes are marked by large dots and small circles respectively. The refinement parameter N_{add} is taken equal to 3 here.

3.2.3 The BEM-STDG method

Collecting the vectors $[u_T]$ and $[v_T]$ for $T \in \mathcal{T}$ in column-wise vectors $[u]$ and $[v]$ respectively, and expressing $\left[p_T^{\#}\right]$ and $\left[q_T^{\#}\right]$ from (32), we form by means of an assembly process, detailed below, the square matrix $[A]$ and colum-wise vector $[b]$ through the following identifications

$$[v]^\top [A] [u] = a(u,v), \quad [v]^\top [b] = Lv.$$

We are hence led to solve the symmetric linear system

$$[A] [u] = [b] .$$

Clearly, $[A]$ is also a sparse matrix in the meaning that any two degrees of freedom which belong to two interior elements not sharing a common face are not connected.

3.2.4 The assembly process

It is helpful in the assembly process to express the above bilinear and linear forms in terms of local forms related to each element T of the mesh $\mathcal{T}$

$$a(u,v) = \sum_{T\in\mathcal{T}} \sum_{F\subset\partial T} a_{F,T}(u,v), \qquad Lv = \sum_{T\in\mathcal{T}} \sum_{F\subset\partial T} L_{F,T} v. \tag{33}$$

However, some additional notation and observations are required before the explicit expressions of these local forms can be obtained.

When F is an interior edge/face shared by T and L, defining similarly as in Eq. (25) by p_L and q_L the dual variables related to L, the integrals on F involved in $a(u,v)$ can be written in a simpler form

$$\begin{aligned} \int_F (\{\!\{u\}\!\}[\![a\nabla v]\!] + [\![a\nabla u]\!]\{\!\{v\}\!\} - \{\!\{a\nabla u\}\!\}\cdot[\![v]\!] - [\![u]\!]\cdot\{\!\{a\nabla v\}\!\})\, ds \\ = \int_F (u_T q_L + u_L q_T + p_T v_L + p_L v_T)\, ds, \end{aligned} \tag{34}$$

$$\int_F (\alpha[\![u]\!][\![v]\!] + \beta\nabla_\top[\![u]\!]\cdot\nabla_\top[\![v]\!])\,ds = \int_F \alpha\,(u_T-u_L)\,v_T + \beta\nabla_\top\,(u_T-u_L)\cdot\nabla_\top v_T ds + \int_F \alpha\,(u_L-u_T)\,v_L ds + \beta\nabla_\top\,(u_L-u_T)\cdot\nabla_\top v_L ds, \tag{35}$$

$$\int_F \gamma[\![a\nabla u]\!][\![a\nabla v]\!]ds = \int_F \gamma\,(p_T+p_L)\,q_T ds + \int_K \gamma\,(p_L+p_T)\,q_L ds. \tag{36}$$

In this way, generically denoting by L the element sharing face F with current element T when $F\in\mathcal{F}_I$, the contribution $a_{F,T}(u,v)$ to the global bilinear form $a(u,v)$ reads

$$\begin{aligned} a_{F,T}(u,v) = &\int_F (p_T v_L + u_L q_T)\,ds \\ &+\int_F (\alpha u_T\,(v_T-v_L) + \beta\nabla_\top u_T\cdot\nabla_\top\,(v_T-v_L) + \gamma\,(p_T+p_L)\,q_T)\,ds. \end{aligned} \tag{37}$$

The expressions of $a_{F,T}(u,v)$ and $L_{F,T}v$ for $F\in\mathcal{F}_\partial$ are obtained in a straightforward way by using the appropriate integral according to the involved part of $\partial\Omega$ and substituting p_T and q_T for respectively $\left(\frac{1}{\varrho_T}\nabla u\right)|_T\cdot\boldsymbol{n}_T$ and $\left(\frac{1}{\varrho_T}\nabla v\right)|_T\cdot\boldsymbol{n}_T$.

Remark It is very important to note that if $\gamma=0$, that is, when the variational formulation involves no penalty on the matching of the dual variables, only p_T and q_T are involved in the expressions of the local forms but neither those p_L nor q_L related to an adjacent element L. Boundary element matrix $\left[D_T^{\#}\right]$ can therefore be computed only at the level of the assembly of element T and has not to be stored.

4 Validation of the numerical method

We begin with the statement of a problem, which involves long-range wave propagation in a typical way. This problem will provide us with a good guideline for measuring the level of "pollution effect" occuring in any numerical solution of the problem. We will hence be able to compare the performances of the BEM-STDG method with the usual polynomial IPDG one. Prior to that, we first give some numerical results confirming the importance of an accurate approximation of the DtN operator, just as was previously mentionned.

4.1 The boundary-value problem

We consider the following example inspired from the wave propagation in a duct with rigid walls as presented in [27]

$$\begin{cases} \Delta u + \kappa^2 n^2 u = 0 \text{ in } \Omega, \\ u(0,y)=1,\ \ \partial_x u(2L,y) - i\kappa u(2L,y) = 0,\ 0<y<H, \\ \partial_y u(x,0) = \partial_y u(x,H) = 0,\ 0<x<2L, \end{cases} \tag{38}$$

set in

$$\Omega = \left\{(x,y)\in\mathbb{R}^2;\ 0<x<2L,\ 0<y<H\right\}, \tag{39}$$

(see FIG. 5) where κ is constant and n is the piecewise constant function given by

$$n = \begin{cases} 1 \text{ for } |x-L| > D, \\ n_0 \text{ for } |x-L| < D. \end{cases} \tag{40}$$

Comparatively with the problem considered in [27], we added a Dirichlet boundary condition on the inlet boundary. In this way, we deal with the three kinds of boundary conditions since we additionally have Neumann and Fourier-Robin boundary conditions on respectively the rigid walls and the outlet boundary. Moreover here, it is possible to consider a non homogeneous duct by choosing n_0 constant but $\neq 1$.

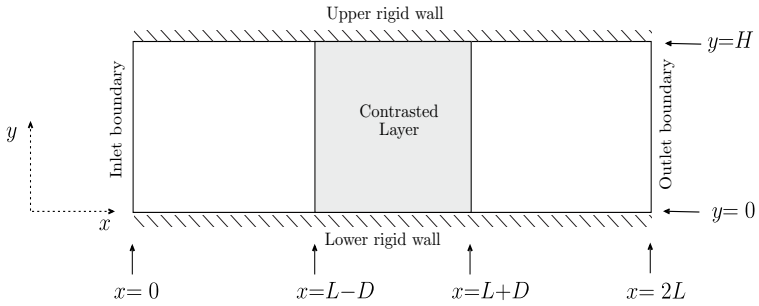

Figure 5: Geometry of the inhomogeneous duct with rigid walls.

Indeed, the solution to this problem is independent of y and can be expressed in terms of four parameters: R, T, R_D, and T_D as follows

$$u(x,y) = \begin{cases} T_D e^{i\kappa n(L-D)x} + R_D e^{-i\kappa n(L-D)x}, & \text{for } |x-L| < D, \\ (1-R)\, e^{i\kappa x} + R e^{-i\kappa x}, & \text{for } x < L-D, \\ T e^{i\kappa x}, & \text{for } x > L+D. \end{cases} \tag{41}$$

Parameters R, T, and R_D can be expressed in terms of T_D through

$$\begin{cases} e^{-i\kappa n_0 D} R_D = \frac{n_0-1}{n_0+1} T_D e^{i\kappa n_0 D}, \; e^{i\kappa L} T = \frac{2n_0}{n_0+1} e^{i\kappa(n_0-1)D} T_D, \\ e^{-i\kappa L} R = -\frac{n_0-1}{2} e^{-i\kappa(n_0+1)D} \left(1 - e^{4i\kappa n_0 D}\right) T_D, \end{cases} \tag{42}$$

which itself is given by

$$T_D = \frac{2e^{i\kappa n_0 D}}{(n_0+1)\, e^{-i\kappa(L-D)} \left(1 - e^{4i\kappa n_0 D} \frac{(n_0-1)^2}{(n_0+1)^2}\right) - (n_0-1)\, e^{i\kappa(L-D)} \left(1 - e^{4i\kappa n_0 D}\right)}. \tag{43}$$

To test the robusteness of the BEM-STDG method relatively to long-range propagation, we mainly limit ourselves to the simpler case where $n_0 = 1$. Then, only T and R remain meaningful and have the following values

$$T = 1, \; R = 0. \tag{44}$$

The structured interior mesh, which is used for these tests, is depicted in FIG. 6. This mesh is characterized by two positive integers $N = 2L$ and $M = H$. In all these tests, κ is taken equal to π, so that the unit length is a half-wavelength. This automatically ensures that the local Dirichlet problem for the Laplace equation is well-posed in each element of the interior mesh.

We use the following errors for characterizing the accuracy of the numerical results:

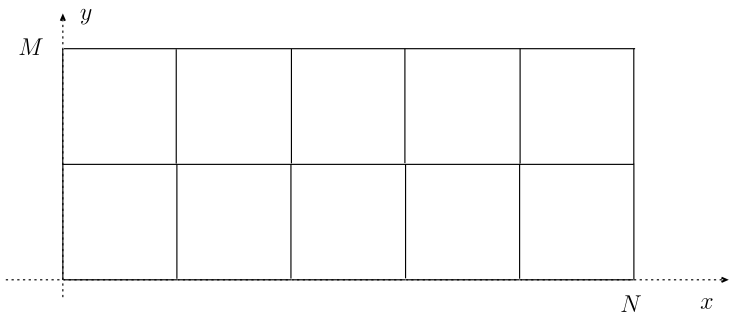

Figure 6: Structured interior mesh used for most of the numerical experiments

- Maximum global error

$$\mathrm{Err}_\infty = 100 \frac{\max_{(x_m,y_m)} |u(x_m,y_m) - u_m|}{\max |u(x,y)|} \tag{45}$$

where u_m is the nodal value at node (x_m, y_m) of the solution delivered by the BEM-STDG method;

- Error on the transmitted wave

$$\mathrm{Err}_\mathrm{T} = 100\,|T - T_\mathrm{comp}| \tag{46}$$

where T is the coefficient, given above, characterizing the solution for $x > L - D$, and T_comp is its approximate value obtained from the numerical simulation;

- Error on the reflected wave

$$\mathrm{Err}_\mathrm{R} = 100\,|R - R_\mathrm{comp}| \tag{47}$$

obtained similarly to Err_T.

4.2 Approximation of the DtN operator on refined meshes

The plots in FIG. 7 depict the maximum error in % for a duct having a length of 500 wavelengths versus the number N_add of segments in which is subdivided each segment of the skeleton mesh.

In all the succeeding text, we characterize each skeleton mesh by the number of nodes per wavelength instead of the meshsize h of the skeleton mesh. The reasons behind the choice of this parameter will be detailed below. For instance, for the BEM, used in this experiment, whose shape functions are polynomials of degree 4, 24 nodes per wavelength correspond to a meshsize $h = 1/3$, that is, 3 segments per half-wavelength, and 16 nodes per wavelength with $h = 1/2$, that is, 2 segments per half-wavelength.

Parameters $\alpha = \beta = 1.0\ 10^2$, $\gamma = 0$, and $\delta = 0$ have been specified empirically. Actually, the method has a low sensitivity relatively to these parameters as soon as α and β are taken sufficiently large, greater than $1.0\ 10^2$ and less than $1.0\ 10^7$, and γ is sufficiently small, set here at zero. It is worth recalling that this choice for γ has a strong impact on the assembly process.

The plots in FIG. 7 clearly demonstrate that a better approximation of the DtN operator greatly reduces the "pollution effect". Below $N_\mathrm{add} = 3$, there has been absolutely no advantage to use 24 instead of 16 nodes per wavelength.

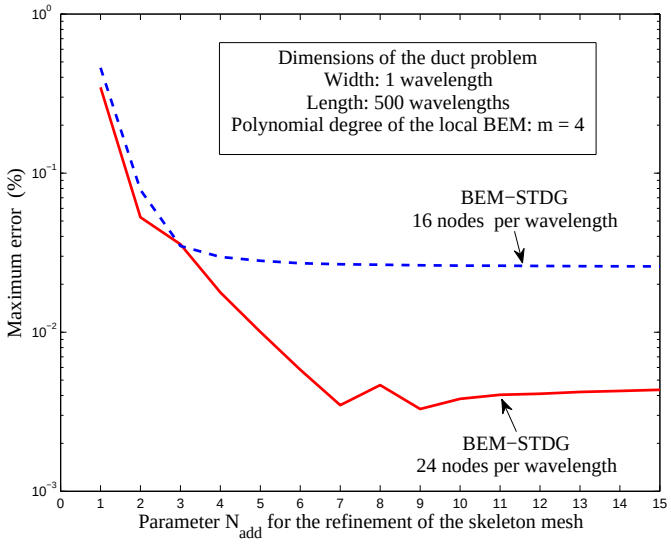

Figure 7: Maximum error in % versus N_{add}

4.3 Validation of the BEM-STDG method

We first validate the BEM-STDG method on two problems of small size. The first one concerns the duct problem considered above and the second one is related to the approximation of an evanescent wave.

4.3.1 A duct problem of small size

We consider the above duct problem for the following data:

- $\kappa = \pi$,
- length of the duct: $2L = 10$ half-wavelengths , width of the duct: $H = 2$ half-wavelengths,
- thickness of the contrasted layer: 4 half-wavelengths ($D = 2$) and its refractive index relatively to the rest of the duct: $n_0 = 2$.

The interior mesh of the duct is depicted in FIG. 8. The two vertical straight lines define the boundary of the contrasted layer.

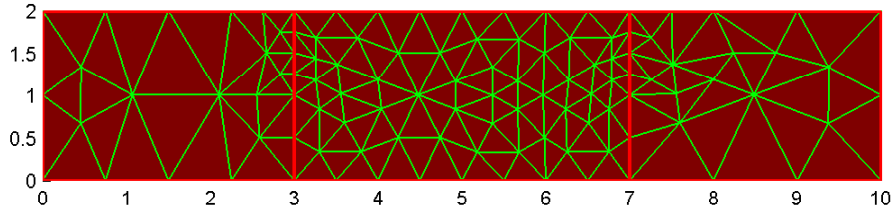

Figure 8: The interior mesh used for solving the small size duct problem.

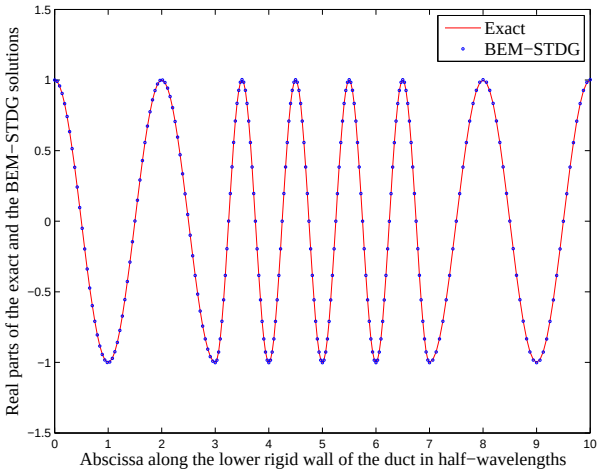

Figure 9: Real parts of the exact and the BEM-STDG solutions for the considered example of the duct problem.

The parameters used for the BEM-STDG method are the following:

- Mesh size of the interior mesh outside the contrasted layer: $h_{\max} = 1$,
- Mesh size of the interior mesh inside the contrasted layer: $h_{\text{layer}} = 0.5$,
- Number of segments per edge of the interior mesh to get the skeleton mesh: 16,
- Number of added segments for the approximation of the DtN operator: $N_{\text{add}} = 4$,
- Polynomial degree used in the BEM: $m = 1$.

The plots in FIG. 9 depict the real parts of the exact and computed solutions on the nodes located on the lower rigid wall $\{y = 0\}$ of the duct. The two curves cannot be distinguished.

The following errors, which are all less than 1 %, validate the BEM-STDG method:

- Maximum error: $\text{Err}_\infty = 0.4$ %;
- Transmitted wave: $\text{Err}_\text{T} = 0.06$ %;
- Reflected wave: $\text{Err}_\text{R} = 0.3$ %.

4.3.2 Approximation of an evanescent mode

Now, we test the ability of the BEM-STDG method to correctly approximate evanescent waves. For this case too, we adapt the conditions leading to an evanescent mode in [27]. We thus consider the same duct geometry than for the previous example with the same wave number $\kappa = \pi$ but we now assume that the duct is homogeneous, that is, $n_0 = 1$, and take

$$u(0, y) = \cos(2\pi y), \ 0 < y < 2, \tag{48}$$

for the data involved in the Dirichlet boundary condition on the inlet boundary. To ensure that the exact solution is the second evanescent mode

$$u(x, y) = \cos(2\pi y) \exp\left(-\sqrt{3}\pi x\right), \tag{49}$$

it is enough to take the following transparent boundary condition on the outlet boundary

$$\left(\partial_x u + \sqrt{3}\pi u\right)(2L, y) = 0,\ 0 < y < 2. \tag{50}$$

We used a interior mesh with $h_{\max} = 0.5$ and, as in the above example, we took 16 segments per edge for the skeleton mesh, $N_{\text{add}} = 4$ for the refinement of the skeleton mesh for the local computation of the DtN operator. Only the maximum error remains meaningful

$$\text{Err}_\infty = 0.4\ \% \tag{51}$$

and is similar to the case of propagative mode. The plot depicted in FIG. 10 shows that the exponential decay of the mode is well reproduced by the solution obtained from the BEM-STDG numerical scheme.

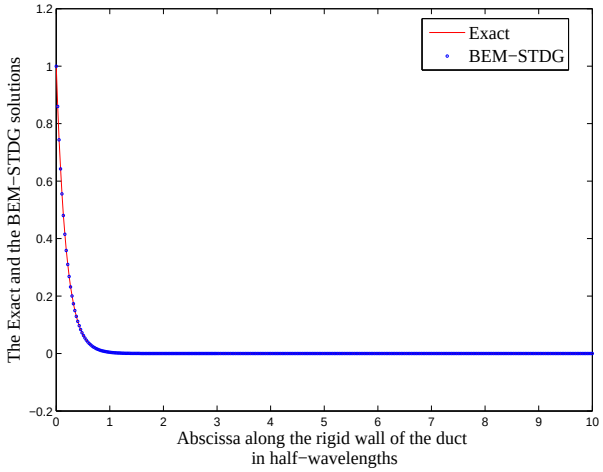

Figure 10: Exact and computed evanescent mode along the lower rigid wall of the duct.

4.4 Long-range propagation

Now, we come to the main motivation for considering this BEM-STDG method: its ability to reduce the "pollution effect" and hence to perform correct numerical simulations of long-range propagation. Toward this end, we consider the case of the above homogeneous duct together with the structured mesh given there. We compare the maximum global errors in % defined earlier versus the length of the duct for the BEM-STDG method with a more conventional polynomial IPDG method (cf., for example, [15]).

It was not easy to find a common basis for comparing the two methods since the accuracy of the overall solution of the BEM-STDG method is mainly based on two meshes: the interior and the skeleton ones, and the polynomial IPDG method uses a usual structured finite element mesh in triangles only. Anyway, the following background seems to be a good basis for this comparison:

- use polynomial local approximations of the same degree for both the BEM-STDG and the polynomial IPDG method;

- assume that the degrees of freedom of the IPDG method are the nodes of the corresponding Lagrange finite element method; then characterize each of these two methods by the density of nodes along each edge (number of nodes per wavelength). For instance, for a polynomial IPDG method constructed on a structured mesh in isosceles rectangular triangles whose length of a right-angle side is $1/N_h$, and for a skeleton mesh built on the structured mesh given in FIG. 6 with N_h segments along each edge, the density, characterizing both the two methods for polynomial shape functions of degree m, will be $2mN_h$.

This error, as a function of the length of the duct, generally fits well with a straight line, at least for large enough lengths. The Least Square Grow Rate (LSGR) is the slope of this straight line, which is obtained by the least square method. It is used as an indicator for the impact of the "pollution effect". Below, we successively compare the two methods from low degree polynomial approximations corresponding to $m = 1$ to high degree ones corresponding to $m = 4$ for various densities of nodes per wavelength and for ducts with length up to 500 wavelengths.

4.4.1 Lowest polynomial degree

For the lowest polynomial degree $m = 1$, the BEM-STDG method widely outclasses the usual polynomial IPDG method. The error of the latter even with a double density of nodes per wavelength is 10 times higher. To be able to plot the error curves corresponding to the two methods in FIG. 11, we have had to use two axes at two different scales. Clearly, as indicated by the reported LSGR, the improvement gained by the BEM-STDG method is mainly due to a much better reduction of the pollution effect.

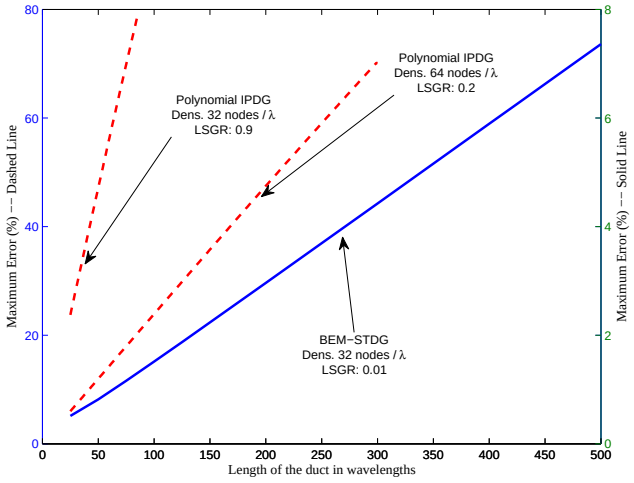

Figure 11: Maximum error in % for polynomial approximations of degree $m = 1$. The left y-axis corresponds to the error curves of the IPDG method and the right y-axis to the BEM-STDG method.

4.4.2 Higher polynomial degrees

For polynomial degrees from $m = 2$ up to $m = 4$, we have done three benchmark tests: the nearest densities to respectively one, one and half, and two times the rule of tumb of 12 nodes per wavelength.

Polynomial degree	Density (nodes / λ)	Method	Error	LSGR
$m = 2$	12	IPDG	72 %	$4.1\ 10^{-1}$
		BEM-STDG	22 %	$4.3\ 10^{-2}$
	16	IPDG	67 %	$1.3\ 10^{-1}$
		BEM-STDG	5.6 %	$1.1\ 10^{-2}$
	24	IPDG	13 %	$2.7\ 10^{-2}$
		BEM-STDG	0.8 %	$1.5\ 10^{-3}$
$m = 3$	12	IPDG	19 %	$3.7\ 10^{-2}$
		BEM-STDG	1.6 %	$3.0\ 10^{-3}$
	18	IPDG	1.7 %	$3.5\ 10^{-3}$
		BEM-STDG	0.1 %	$1.0\ 10^{-4}$
	24	IPDG	0.3 %	$6.2\ 10^{-4}$
		BEM-STDG	0.02 %	$-2.6\ 10^{-10}$
$m = 4$	8	IPDG	1.8 %	$3.9\ 10^{-3}$
		BEM-STDG	10.4 %	$2.0\ 10^{-2}$
	16	IPDG	0.17 %	$3.0\ 10^{-4}$
		BEM-STDG	0.02 %	$4.3\ 10^{-6}$
	24	IPDG	0.007 %	$1.3\ 10^{-5}$
		BEM-STDG	0.003 %	$3.0\ 10^{-12}$

Table 1: Maximum error in % for a duct of 500 wavelengths and Least Square Grow Rate of the error as a function of the length of the duct.

The results are reported in TAB. 1 and the most featuring of these are depicted in FIG. 12, FIG. 13, FIG. 14, and FIG. 15. The negative LSGR for $m = 3$ and a density of 24 nodes per wavelength is certainly due to rounding errors (see also FIG. 13 below).

All these benchmark tests, except the one corresponding to a polynomial degree $m = 4$ and a density of 8 nodes per wavelength depicted in FIG. 14, confirm that the BEM-STDG method is able to reduce the pollution effect much more efficiently than the usual polynomial IPDG method. The case where the BEM-STDG method succeeded less well than the polynomial IPDG method is that where the density was only of 8 nodes per wavelength, hence being less than the usual rule of thumb of 12 nodes per wavelength. This suggests that the BEM-STDG method requires a minimal density of nodes to be efficient.

It must also be noticed that the BEM-STDG method succeeded to practically rub out the "pollution effect" up to 500 wavelengths for polynomial approximations $m = 3$ and $m = 4$ with 24 nodes per wavelength (see FIG. 13 and FIG. 15), contrary to the IPDG method for which this error continues to feature even at a low level in some cases.

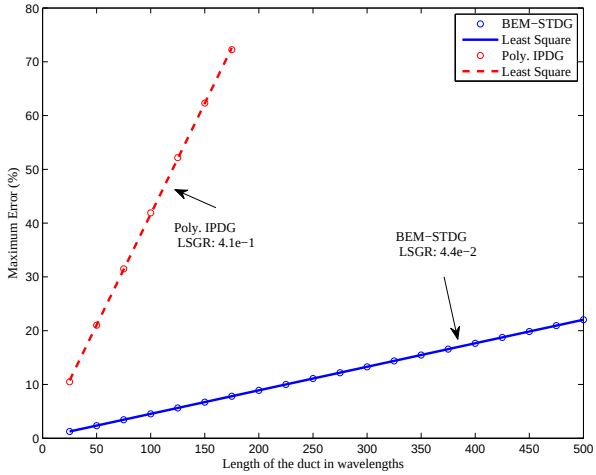

Figure 12: Maximum error in % for polynomial approximations of degree $m = 2$ and a density of 12 nodes per wavelength.

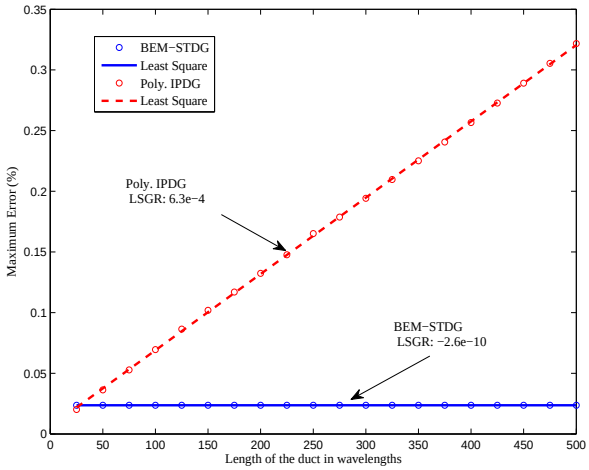

Figure 13: Maximum error in % for polynomial approximations of degree $m = 3$ and a density of 24 nodes per wavelength.

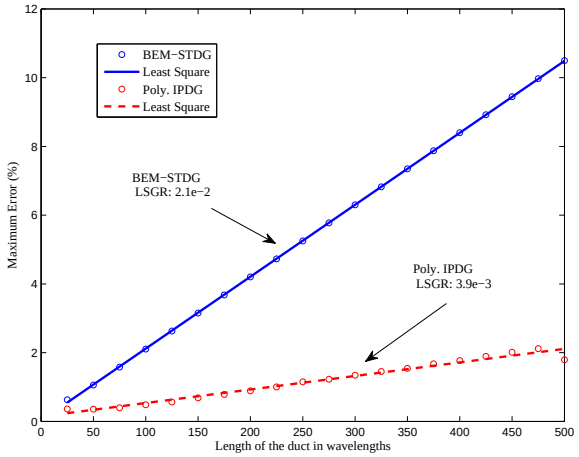

Figure 14: Maximum error in % for polynomial approximations of degree $m = 4$ and a density of 8 nodes per wavelength.

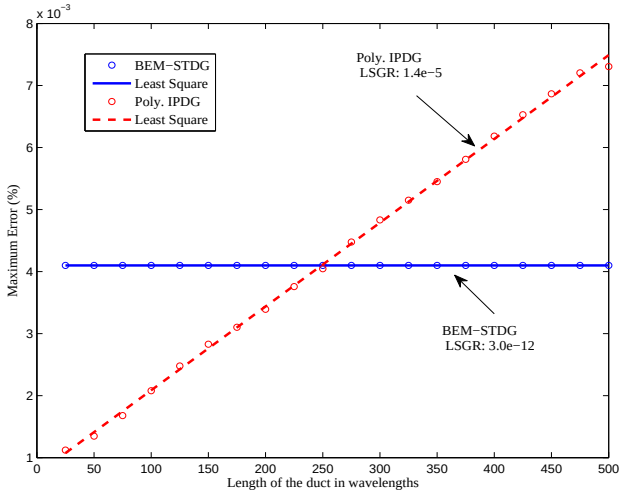

Figure 15: Maximum error in % for polynomial approximations of degree $m = 4$ and a density of 24 nodes per wavelength.

5 Concluding remarks

At first, it is worth stressing the outstanding stability of the BEM-STDG method relatively to the penalty parameters. All the results were obtained using the same set of parameters. Generally, for usual IPDG methods, these parameters have to be tuned according to geometrical features of the neighboring elements and the polynomial degree of the local shape functions.

On the other hand, this study has confirmed the expected property that a TDG method, whose local shape functions are obtained by means of a BEM, considerably reduces the so-called "pollution effect" instabilities. It was even shown that it is possible to completely rub out the "pollution effect" by slightly refining the skeleton mesh and using a BEM of moderate polynomial degree. It should be noted that these excellent performances have been obtained through an extremely careful tuning of the BEM method, but done once for all when implementing the BEM code. In particular, the most difficult part of this task is an elaborate way for computing the involved singular and regular integrals. A complete description of the procedure used to this effect will be given elsewhere. The accurate computation of the approximation of the DtN operator must be also noticed.

The current study gives also rise to several questions:

- Is it possible to replace the BEM solution by the approximation of the DtN operator through a suitable FEM?
- Is it possible to confirm the excellent reduction of the "pollution effect" observed for the duct problem by a study of the dispersion of the related numerical scheme, following the approach described in [1], or at least numerically as in [19]?
- Does the UWVF can be dealt with using a similar way to proceed based on a BEM for building the local approximating functions?
- Is it possible to theoretically justify the stability of the method relatively to the size of the propagation domain?

All these issues will be studied in forthcoming papers.

References

[1] M. Ainsworth. Dispersive and dissipative behaviour of high order discontinuous Galerkin finite element methods. *Journal of Computational Physics*, 198:106–130, 2004.

[2] M. Ainsworth, P. Monk, and W. Muniz. Dispersive and dissipative properties of discontinuous Galerkin finite element methods for the second-order wave equation. *Journal of Scientific Computing*, 27(1–3):5–40, 2006.

[3] M. Amara, H. Calandra, R. Dejllouli, and M. Grigoroscuta-Strugaru. A stable discontinuous Galerkin-type method for solving efficiently Helmholtz problems. *Computers and Structures*, 106–107:258–272, 2012.

[4] D. N. Arnold. An interior penalty finite element method with discontinuous elements. *SIAM J. Num. Analysis*, 19(4):742–760, 1982.

[5] D. N. Arnold, F. Brezzi, B. Cockburn, and L. D. Marini. Unified analysis of discontinuous Galerkin methods for elliptic problems. *SIAM J. Num. Analysis*, 39(5):1749–1779, 2002.

[6] A. Bendali and M. Fares. Boundary integral equations methods in acoustics. In F. Magoules, editor, *Computer Methods for Acoustics Problems*, chapter 1, pages 1–36. Saxe-Coburg Publications, Kippen, Stirlingshire, Scotland, 2008.

[7] A. Buffa and P. Monk. Error estimates for the ultra weak variational formulation of the Helmholtz equation. *Mathematical Modelling and Numerical Analysis*, 42(6):925–940, 2008.

[8] J. E. Caruthers, J. C. French, and G. K. Raviprakash. Green function discretization for numerical solution of the Helmholtz equation. *Journal of Sound and Vibration*, 187(4):553–568, 1995.

[9] O. Cessenat. *Application d'une nouvelle formulation variationnelle aux équations d'ondes harmoniques. Problèmes d'Helmholtz 2D et de Maxwell 3D.* PhD thesis, University of Paris XI Dauphine, 1996.

[10] O. Cessenat and B. Després. Application of an ultra weak variational formulation of elliptic pdes to the two-dimensional Helmholtz problem. *SIAM J. Num. Analysis*, 35(1):255–299, 1998.

[11] P. G. Ciarlet. *The Finite Element Method for Elliptic Problems*. North Holland, Amsterdam, 1978.

[12] B. Cockburn, J. Gopalakrishnan, and R. Lazarov. Unified hybridization of discontinuous Galerkin, mixed, and continuous Galerkin methods for second order elliptic problems. *SIAM J. Num. Analysis*, 47(2):1319–1365, 2009.

[13] B. Després. Sur une formulation variationnelle ultra-faible. *Comptes Rendus de l'Académie des Sciences*, Série I 318:939–944, 1994.

[14] E. G. D. do Carmo, G. B. Alvarez, A. F. D. Loula, and F. A. Rochinha. A nearly optimal Galerkin projected residual finite element method for Helmholtz problem. *Comput. Meth. Appl. Mech. Engrg.*, 197:1362–1375, 2008.

[15] X. Feng and H. Wu. Discontinuous Galerkin methods for the Helmholtz equation with large wave number. *SIAM J. Numer. Anal.*, 47(4):2872–2896, 2009.

[16] G. Gabard. Discontinuous Galerkin methods with plane waves for time-harmonic problems. *Journal of Computational Physics*, 225:1961–1984, 2007.

[17] P. Gamallo and R. J. Astley. A comparison of two Trefftz-type methods: The ultraweak variational formulation and the least-squares method, for solving shortwave 2-D Helmholtz problems. *International Journal for Numerical Methods in Engineering*, 71:406–432, 2007.

[18] G. Giorgiani, S. Fernández-Méndez, and A. Huerta. Hybridizable discontinuous Galerkin p-adaptivity for wave propagation problems. *Int. J. Numer. Meth. Fluids*, 72:1244Ũ1262, 2013.

[19] C. Gittelson and R. Hiptmair. Dispersion analysis of plane wave discontinuous methods. *International Journal for Numerical Methods in Engineering*, 98(5):313–323, 2014.

[20] C. J. Gittelson, R. Hiptmair, and I. Perugia. Plane wave discontinuous Galerkin methods: analysis of the h-version. *Mathematical Modelling and Numerical Analysis*, 43:297–331, 2009.

[21] J. S. Hesthaven and T. Warburton. *Nodal Discontinuous Galerkin Methods. Algorithms, Analysis, and Applications*, volume 54 of *Texts in Applied Mathematics*. Springer, Berlin, Heidelberg, 2008.

[22] R. Hiptmair, A. Moiala, and I. Perugia. A survey of Trefftz methods for the Helmholtz equation. Research Report 2015-20, SAM ETH Zurich, 2015. to appear in Springer Lecture Notes on Computational Science and Engineering.

[23] R. Hiptmair, A. Moiola, and I. Perugia. Trefftz discontinuous Galerkin methods for acoustic scattering on locally refined meshes. *Applied Numerical Mathematics*, 79:79–91, 2014.

[24] R. Hiptmair and I. Perugia. Mixed plane wave DG methods. In M. Bercovier, M. J. Gander, R. Kornhuber, and O. Windlund, editors, *Domain decomposition methods in science and engineering XVIII*, Lect. Notes Comput. Sci. Eng. Springer, 2008.

[25] G. C. Hsiao and W. L. Wendland. *Boundary Iintegral Equations*. Springer, Berlin-Heidelberg, 2008.

[26] T. J. R. Hughes. Multiscale phenomena: GreenŠs functions, the Dirichlet-to-Neumann formulation, subgrid scale models, bubbles and the origins of stabilized methods. *Comput. Methods Appl. Mech. Engrg.*, 127:387–401, 1995.

[27] T. Huttunen, P. Gamallo, and R. J. Astley. Comparison of two wave element methods for the Helmholtz equation. *Comm. Numer. Meth. Engrg.*, 25(1):35–52, 2009.

[28] T. Huttunen, J. P. Kaipio, and P. Monk. The perfectly matched layer for the ultra weak variational formulation of the 3D Helmholtz equation. *International Journal for Numerical Methods in Engineering*, 61:1072–1092, 2004.

[29] F. Ihlenburg and I. Babuska. Finite element solution of the Helmholtz equation with high wave number – part i: the h-version of the FEM. *Computers Math. Applic.*, 30(9):9–37, 1995.

[30] Jianming Jin. *The Finite Element Method in Electromagnetics, Second Edition*. John Wiley & Sons, New York, 2002.

[31] L. D. Landau and E. M. Lifschitz. *Fluid Mechanics 2nd edition*, volume 6 of *Landau and Lifschitz: course of theoretical physics*. Elsevier, Amsterdam, reprinted with corrections 2009 edition, 1987.

[32] A. F.D. Loula, G. B. Alvarez, E. G.D. do Carmo, and F. A. Rochinha. A discontinuous finite element method at element level for Helmholtz equation. *Comput. Meth. Appl. Mech. Engrg.*, 196:867–878, 2007.

[33] J. M. Melenk, A. Parsania, and S. Sauter. General DG-Methods for highly indefinite Helmholtz problems. *J. Sci. Comput.*, 57:536–581, 2013.

[34] A. Moiola, R. Hiptmair, and I. Perugia. Plane wave approximation of homogeneous Helmholtz solutions. *Z. Angew. Math. Phys.*, 62:809–837, 2011.

[35] J.-C. Nédélec. *Acoustic and Electromagnetic Equations: Integral Representations for Harmonic Problems*. Springer, Berlin, 2001.

[36] N. C. Nguyen, J. Peraire, F. Reitich, and B. Cockburn. A phase-based hybridizable discontinuous Galerkin method for the numerical solution of the Helmholtz equation. *Journal of Computational Physics*, 290:318–335, 2015.

[37] D. A. Di Pietro and A. Ern. *Mathematical Aspects of Discontinuous Galerkin Methods.* Springer, Berlin Heidelberg, 2012.

[38] B. Pluymers, B. van Hal, D. Vandepitte, and W. Desmet. Trefftz-based methods for time-harmonic acoustics. *Archives for Computational Methods in Engineering*, 14(4):343–381, 2007.

[39] S.W. Rienstra and A. Hirschberg. *An introduction to acoustics.* S.W. Rienstra & A. Hirschberg 2004, 2004. avalaible on line http://www.win.tue.nl/ sjoerdr/papers/boek.pdf.

[40] S. A. Sauter and C. Schwab. *Boundary Element Methods.* Springer-Verlag, Berlin-Heidelberg, 2011.

[41] J. F. Semblat and J. J. Brioist. Efficiency of higher order finite element for the analysis of seismic wave propagation. *Journal of Sound and Vibration*, 231(2):460–467, 2000.

[42] E. Spence. "When all else fails, integrate by parts". An overview of new and old variational formulations for linear elliptic PDEs. In A. Fokas and B. Pelloni, editors, *Unified transform methods for boundary value problems: applications and advances.*, pages 93–159, Philadelphia, 2015. SIAM.

[43] D. Wang, R. Tezaur, J. Toivanen, and C. Ferhat. Overview of the discontinuous enrichment method, the ultra-weak variational formulation, and the partition of unity method for the acoustic scattering in the medium frequency regime and performance comparisons. *International Journal for Numerical Methods in Engineering*, 89:403–417, 2012.

[44] C. H. Wilcox. *Scattering theory for the d'Alembert equation in exterior domains*, volume 442. Springer-Verlag, Berlin, 1975.

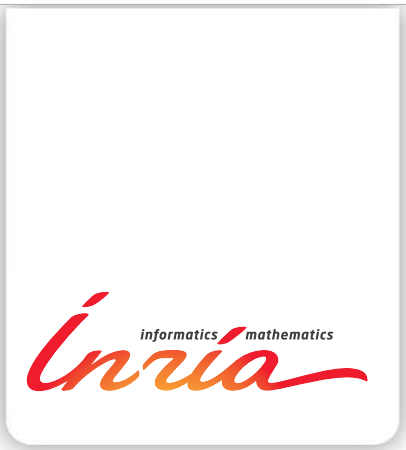

RESEARCH CENTRE
BORDEAUX – SUD-OUEST

200 avenue de la Vieille Tour
33405 Talence Cedex

Publisher
Inria
Domaine de Voluceau - Rocquencourt
BP 105 - 78153 Le Chesnay Cedex
inria.fr

ISSN 0249-6399